Electronic Supplementary Information (ESI)

All-cellulose-derived humidity sensor prepared *via* direct laser writing of conductive and moisture-stable electrodes on TEMPO-oxidized cellulose paper

Luting Zhu, Xiang Li, Takaaki Kasuga, Kojiro Uetani, Masaya Nogi, Hirotaka Koga*

SANKEN (The Institute of Scientific and Industrial Research), Osaka University, 8-1 Mihogaoka, Ibaraki, Osaka 567-0047, Japan.

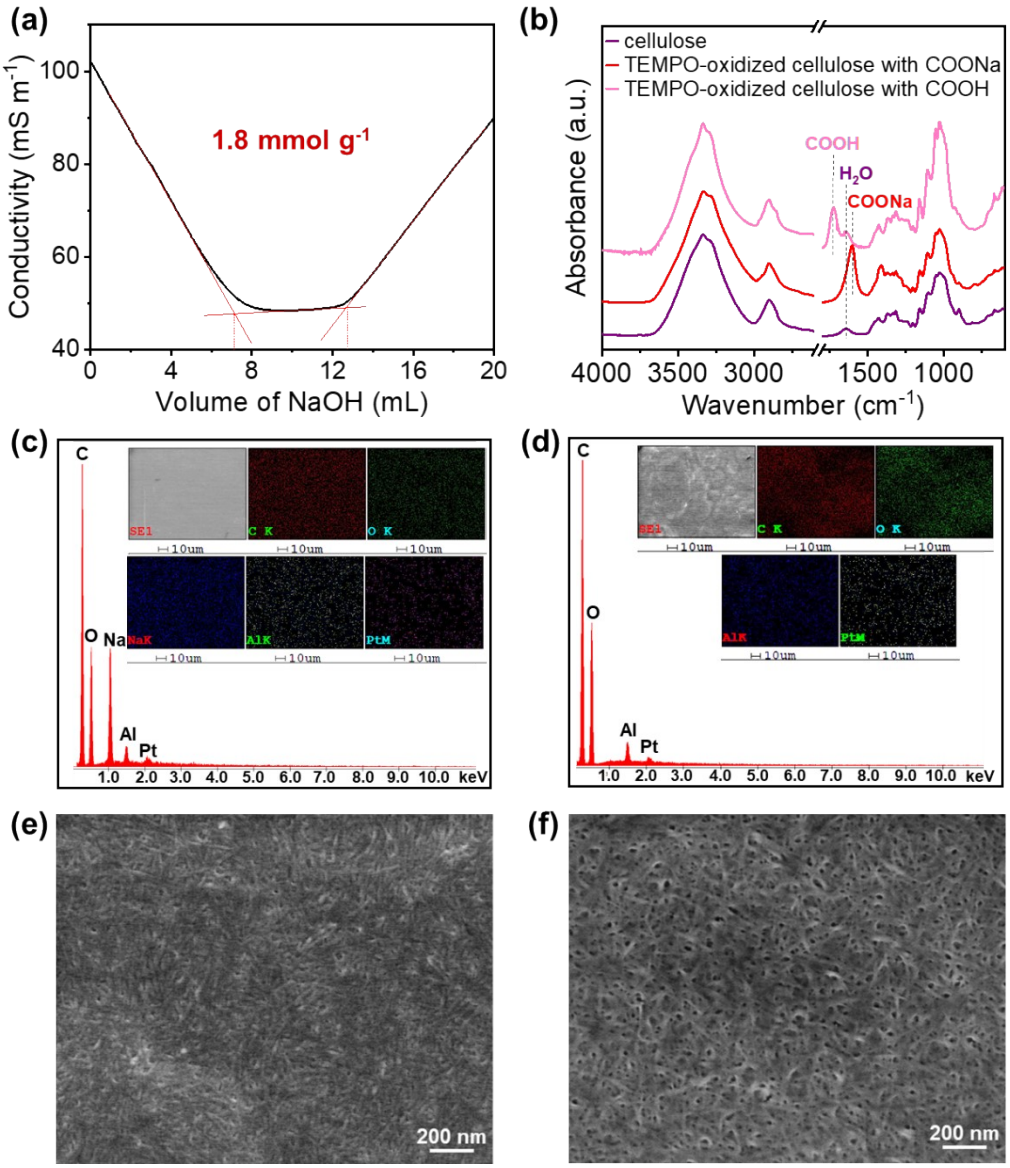

Figure S1 Characterization of TEMPO-oxidized cellulose fibers. (a) Conductometric curve of the titration of TEMPO-oxidized cellulose fibers using NaOH to calculate their carboxylate content, (b) FT-IR spectra of original cellulose fibers (purple) and TEMPO-oxidized cellulose fibers with COONa groups (red) or COOH groups (pink). (c, d) EDX spectra and (e, f) FE-SEM images of TEMPO-oxidized cellulose papers with (c, e) COONa and (d, f) COOH groups.

As shown in **Figure S1a**, the carboxylate content of the TEMPO-oxidized cellulose fibers was measured using a conductometric titration method.[1] A TEMPO-oxidized cellulose fiber suspension was diluted to 0.1–0.15 wt% with distilled water, followed by the addition of 0.01 M NaCl solution (5 mL). Subsequently, the pH of the suspension was

adjusted to 2.5–3.0 by adding 0.5 M HCl. The suspension was then titrated by adding 0.05 M NaOH at a speed of 0.1 mL min^{-1} using an automatic titrator (AUT-701, DKK-TOA Corp., Tokyo, Japan). The carboxylate content (n, mmol g^{-1}) was calculated using the following equation:

$$n = \frac{V \times c}{\omega}$$

where V, c, and ω denote the volume of NaOH solution consumed in the plateau region of the titration profile (**Figure S1a**), concentration of the titrated NaOH solution, and weight of the measured sample, respectively. In this study, the calculated COONa content was approximately 1.8 mmol g^{-1}.

We also performed FT-IR analysis (**Figure S1b**). The peaks at approximately 1605 and 1720 cm^{-1} indicate the existence of COONa and COOH, respectively.[2] Thus, the FT-IR spectra confirmed that COONa groups were introduced into cellulose after TEMPO oxidation, and that the COONa groups could be changed to COOH groups by HCl treatment, which were also consistent with EDX data (**Figure S1c and d**). The Pt and Al elements in the EDX spectra were derived from the sputtered Pt and the Al holder for the FE-SEM observation, respectively. The FE-SEM observation indicated that TEMPO-oxidized cellulose papers with COONa and COOH groups had nanoscale fiber-packed structures (**Figure S1e and f**).

In this paper, all data presented are for TEMPO-oxidized cellulose fibers with COONa groups, except for **Figure S5a–c**.

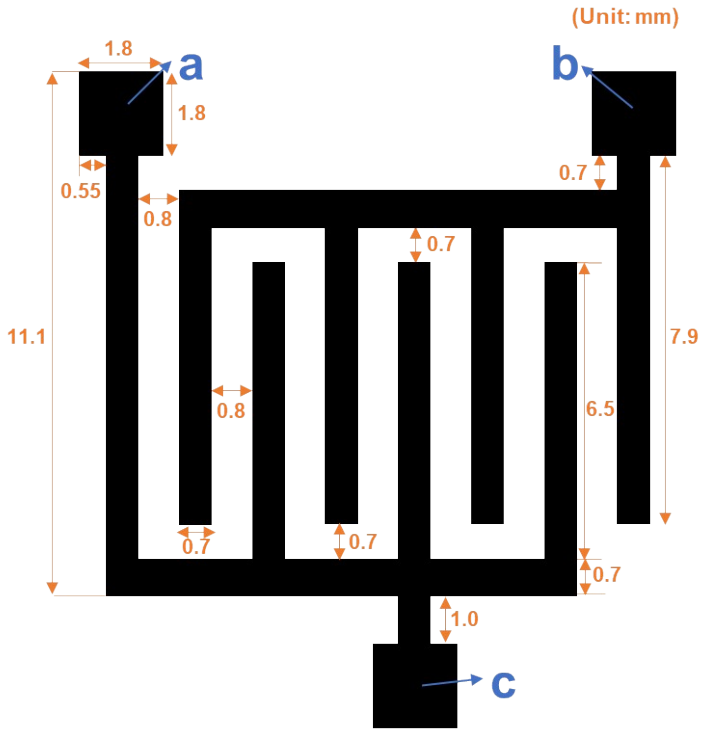

Figure S2 CO_2 laser-irradiation pattern to form interdigitated electrodes used in this study. Probes for measuring the sensing performance of the humidity sensor were placed at points a and b, whereas points a and c were used to evaluate the electrode performance.

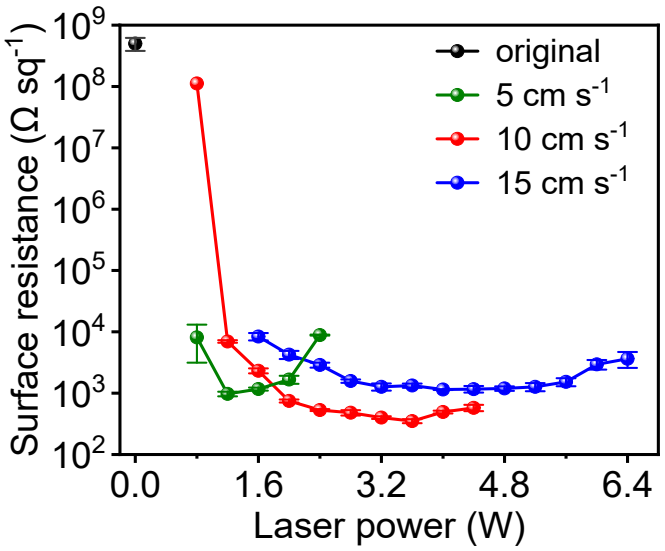

Figure S3 Surface resistance versus CO_2 laser power for the laser-irradiated area on the TEMPO-oxidized cellulose paper at different laser scan rates (measured at a relative humidity of 25%).

The surface resistance of the CO_2 laser-irradiated area was between 10^8 and 10^2 Ω sq^{-1}, depending on the laser irradiation conditions (laser power and scan rate). At each scan speed, the surface resistance initially decreased and then gradually increased with increasing laser power. Slower scan speeds, which equate to longer laser-irradiation times, resulted in increased surface resistance at a relatively low laser power. These results suggest that excess laser energy is undesirable for the preparation of conductive electrodes on TEMPO-oxidized cellulose paper, because partial ablation may occur. For the preparation of conductive (low surface resistance) lines, we adopted a laser scan rate of 10 cm s^{-1} to prepare the humidity sensor.

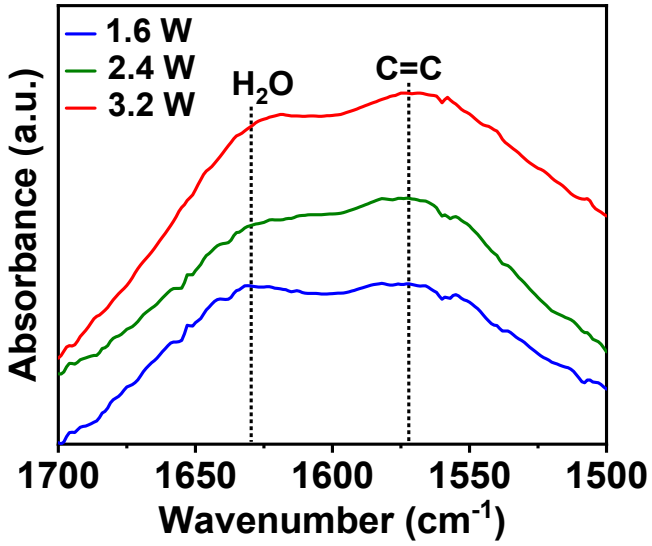

Figure S4 FT-IR spectra of laser-induced electrodes prepared at different laser powers after storing at a relative humidity of 98%.

To analyze the water adsorption behavior of laser-induced electrodes produced at 1.6, 2.4, and 3.2 W, the electrodes were peeled off from the TEMPO-oxidized cellulose paper, and then subjected to FT-IR analyses after storage at high relative humidity (98%) for more than 12 h. For each laser power, an FT-IR peak was observed at approximately 1630 cm^{-1}, which represents physically adsorbed water molecules;[2] in addition, there were no large differences in the intensity ratios of C=C bonds and physically adsorbed water peaks between each electrode. Thus, the water molecules were physically adsorbed onto the laser-induced electrodes, regardless of the irradiated laser power.

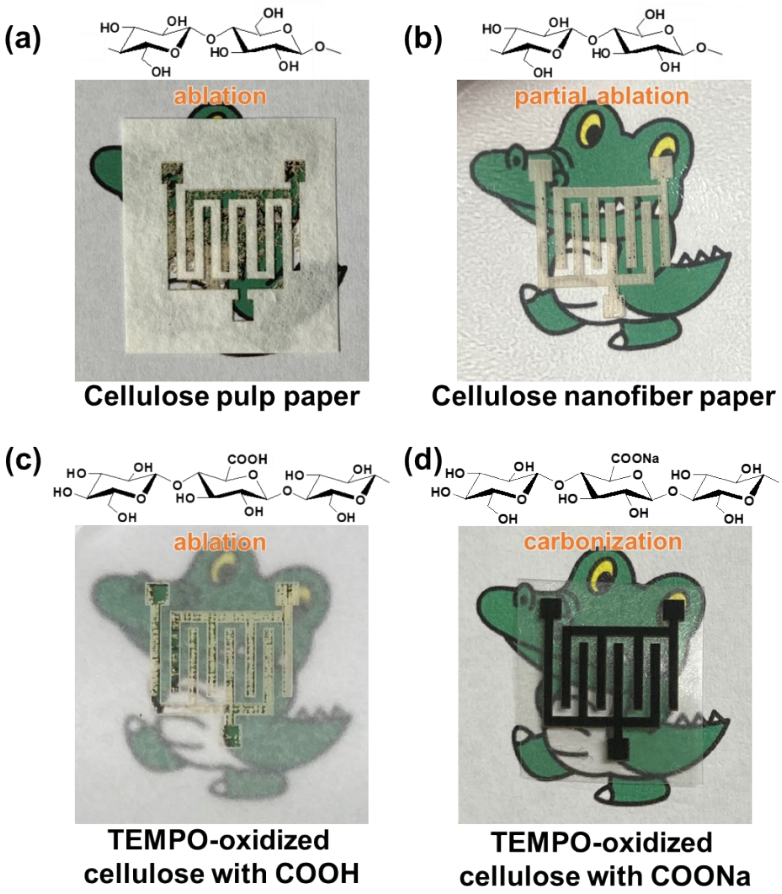

Figure S5 Optical images of different cellulose papers after CO_2 laser irradiation. (a) Cellulose pulp paper, (b) cellulose nanofiber paper, (c,d) TEMPO-oxidized cellulose paper with (c) COOH and (d) COONa groups. Laser power: 3.2 W. Laser scan rate: 10 cm s^{-1}.

Films of cellulose pulp and TEMPO-oxidized cellulose with COOH groups were ablated when subjected to CO_2 laser irradiation (**Figure S5a–c**), indicating that they are not suitable substrates for fabricating laser-induced electrodes. In contrast, the TEMPO-oxidized cellulose with COONa groups was successfully carbonized by CO_2 laser irradiation to form conductive electrodes (**Figure S5d**, see also **Figures 1b and 2**). This phenomenon could be because the presence of the COONa groups improved the yield of carbonaceous materials after CO_2 irradiation of TEMPO-oxidized cellulose (see also **Figure S6**).

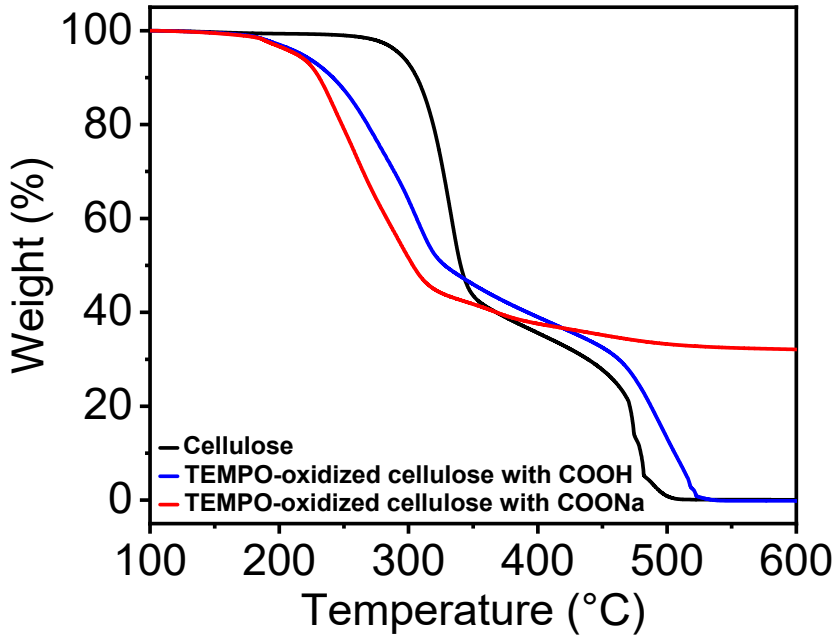

Figure S6 Thermogravimetric curves of different cellulose papers in air.

The thermal decomposition temperature (T_d) of TEMPO-oxidized cellulose with carboxylate (COOH and COONa) groups was lower than that of the original cellulose, because the carboxyl groups degrade at lower temperatures by decarbonation.[3] When heated in air, the weight of the original cellulose and TEMPO-oxidized cellulose with COOH groups reduced to almost 0% by 550 °C, indicating that ablation occurred. However, TEMPO-oxidized cellulose with COONa groups retained approximately 32% of its original weight even at 600 °C. The remaining weight was considerably higher than the weight of Na (approximately 4 wt%) in the material, clearly indicating the existence of carbonaceous materials. The CO_2 laser-induced carbonization of polymeric materials is attributed to the generation of thermal energy (high temperatures) induced by the photothermal effect derived from their lattice vibrations.[4] Thus, these results suggest that the presence of COONa groups in TEMPO-oxidized cellulose improves the yield of carbonaceous materials after CO_2 laser irradiation, thereby facilitating the CO_2 laser-induced formation of conductive electrodes.

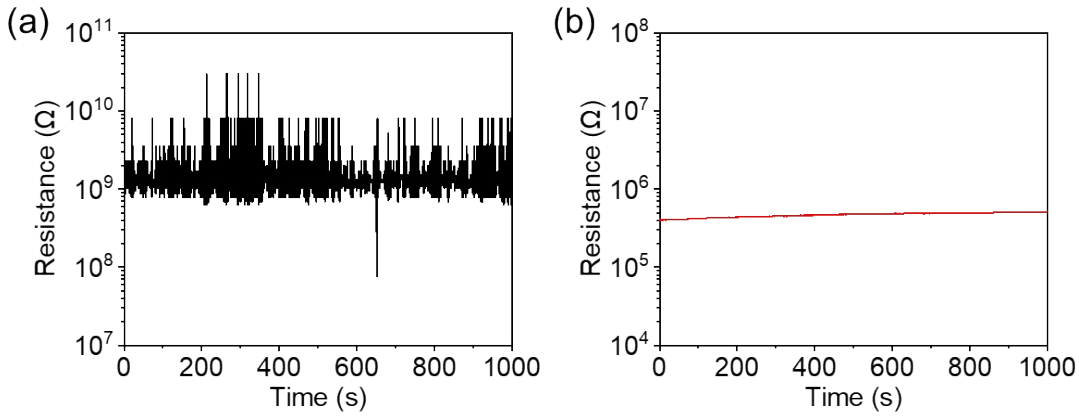

Figure S7 Resistance versus time of TEMPO-oxidized cellulose paper (a) without and (b) with laser-induced electrodes. Laser power: 3.2 W. Laser scan rate: 10 cm s^{-1}. Resistance values were measured at a relative humidity of 65%.

We measured the resistance of the TEMPO-oxidized cellulose paper with COONa groups with and without CO_2 laser-induced interdigitated electrodes. In the absence of interdigitated electrodes, the detected resistance oscillated significantly over time owing to the high resistance of the TEMPO-oxidized cellulose paper with COONa groups (over 10^9 Ω) (**Figure S7a**), leading to considerable difficulty in the stable detection of electrical signals from the humidity sensing material without electrodes. In contrast, the interdigitated electrodes significantly decreased the detected resistance to approximately 10^5 Ω (**Figure S7b**) because of the formation of parallel circuits derived from the interdigitated structures,[5] thus ensuring the stable detection of electrical signals for accurate sensing.

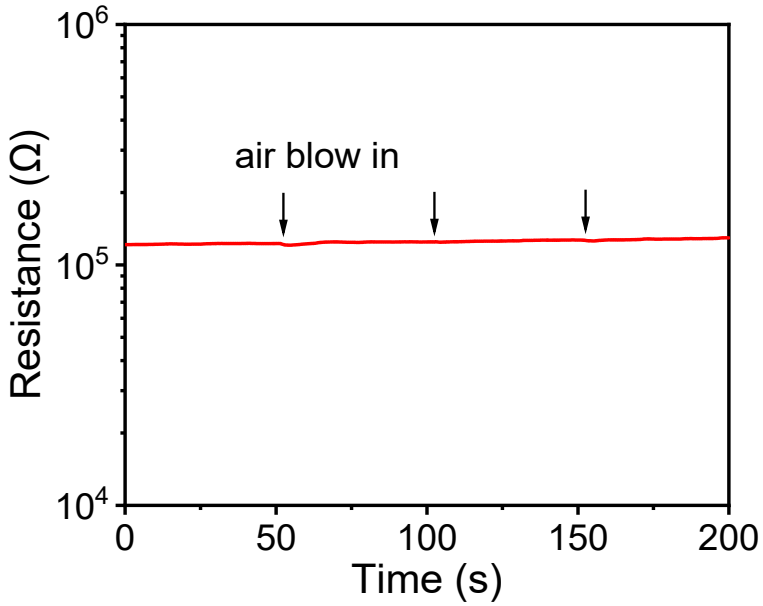

Figure S8 Resistance versus time of all-cellulose-derived humidity sensors upon exposure to air blow. Air blowing time: approximately 3 s. Relative humidity: 80%. The electrodes were prepared at a laser power of 3.2 W.

The resistance of the all-cellulose-derived humidity sensor with electrodes prepared at a laser power of 3.2 W remained almost stable when air was blown onto the surface (**Figure S8**), but changed upon exposure to water vapor (**Figure 3b**). These results indicate that the sensors respond well to the presence of water vapor, thereby enabling humidity sensing performance.

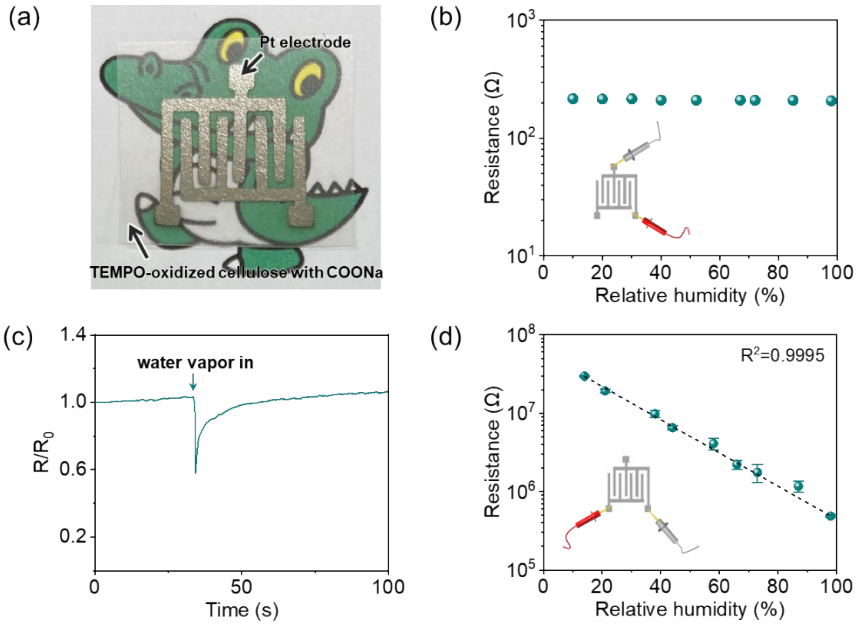

Figure S9 Humidity sensing performances of the sensor consisting of TEMPO-oxidized cellulose paper with COONa groups and sputtered Pt electrodes. (a) Optical image of the sensor, (b) electrical resistivity versus humidity of the Pt electrode, (c) relative resistance (R/R_0) versus time of the sensor with Pt electrodes upon exposure to water vapor from a humidifier, (d) resistance versus relative humidity of the sensor with Pt electrodes. All performance testing was conducted at room temperature.

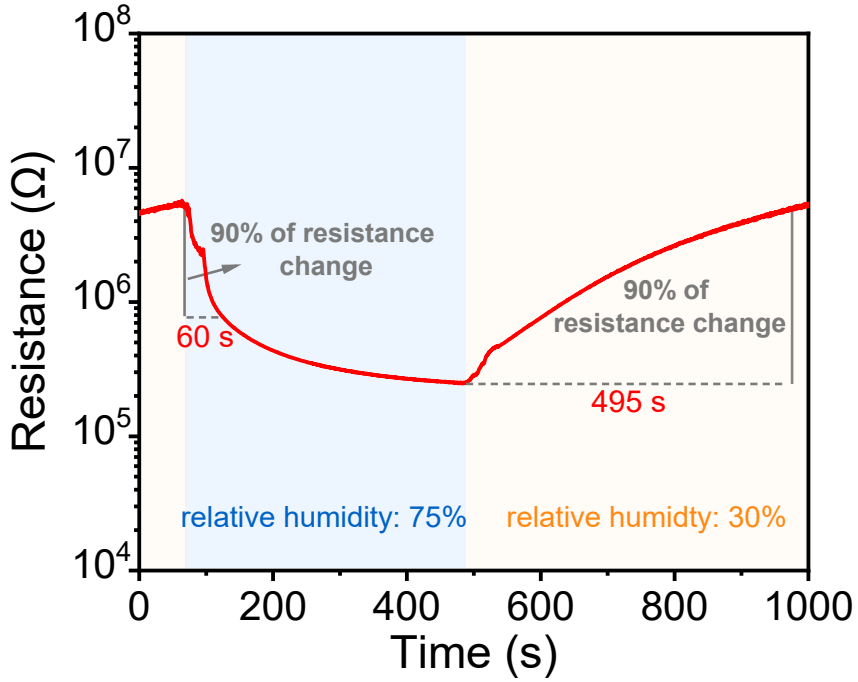

Figure S10 Response and recovery curve of the all-cellulose-derived humidity sensor. The laser-induced electrodes were formed at laser-irradiation power and scan rate of 3.2 W and 10 cm s^{-1}, respectively.

The response and recovery times are defined as the time required to reach 90% of the change of sensor resistance.[6] As shown in **Figure S10**, the response and recovery times of the all-cellulose-derived humidity sensor were estimated as 60 and 495 s, respectively.

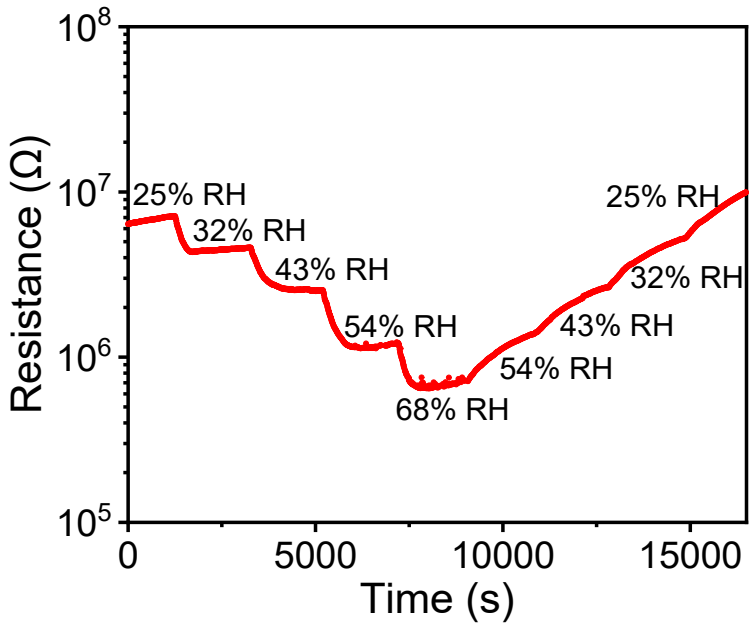

Figure S11 Real-time response and recovery curve of all-cellulose-derived humidity sensor in the relative humidity (RH) range from 25 to 68%. The electrodes were prepared at a laser power of 3.2 W.

The real-time response recovery curve of the all-cellulose-derived humidity sensor was measured in the RH range from 25 to 68% by using a bench-top type temperature and humidity chamber. The resistance values of the humidity sensor were relatively unstable at 68% RH, possibly due to unstable humidity conditions in the chamber. Owing to the large size of the chamber (W400 mm×H400 mm×D400 mm), it required time to modulate the humidity, thereby increasing the response and recovery times of the sensor in this system. Nevertheless, the resistance value of the sensor showed real-time response and recovery upon the humidity change, which was consistent with the hysteresis curve of the humidity sensor (see also **Figure 3f**).

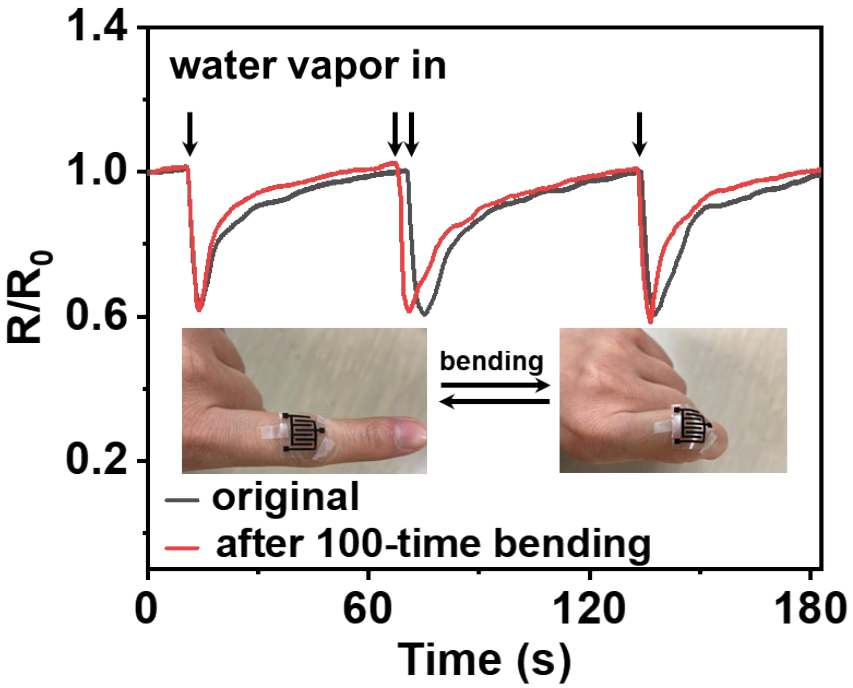

Figure S12 Humidity sensing performance of all-cellulose-derived humidity sensor before (gray) and after (red) 100-time bending (RH: 24%). The electrodes were prepared at a laser power of 3.2 W.

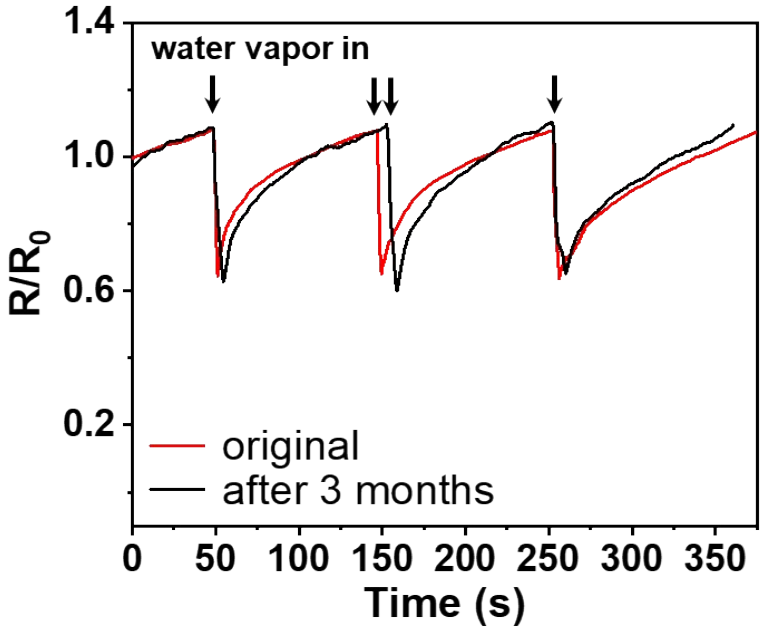

Figure S13 Humidity sensing performance of all-cellulose-derived humidity sensor before (red) and after (black) storing for 3 months (RH: 50%). The electrodes were prepared at a laser power of 3.2 W.

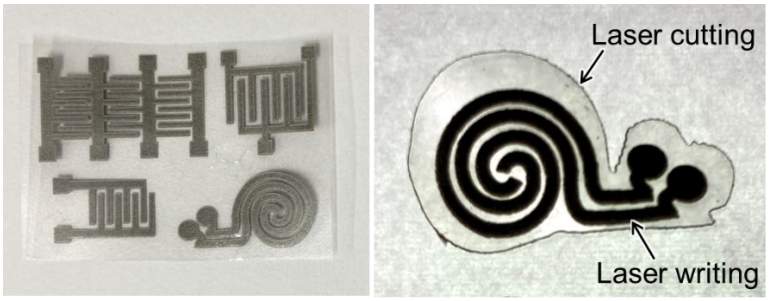

Figure S14 Versatile configuration design of all-cellulose-derived humidity sensors with electrode and shape patterning by CO_2 laser processing. Optical images of the backside of several humidity sensors (left), and the surface of a sensor designed with a snail-like configuration (right).

The CO_2 laser irradiation process can be used to fabricate various patterned electrodes on the surface of the TEMPO-oxidized cellulose paper (thickness: approximately 70 μm). Because CO_2 laser-induced carbonization does not extend to the backside of the paper (**Figure S14**, left), the backside of the sensor remains electrically insulating. The laser process can also be used to cut the paper into a desired shape, allowing for a versatile configuration of humidity sensors (**Figure S14**, right).

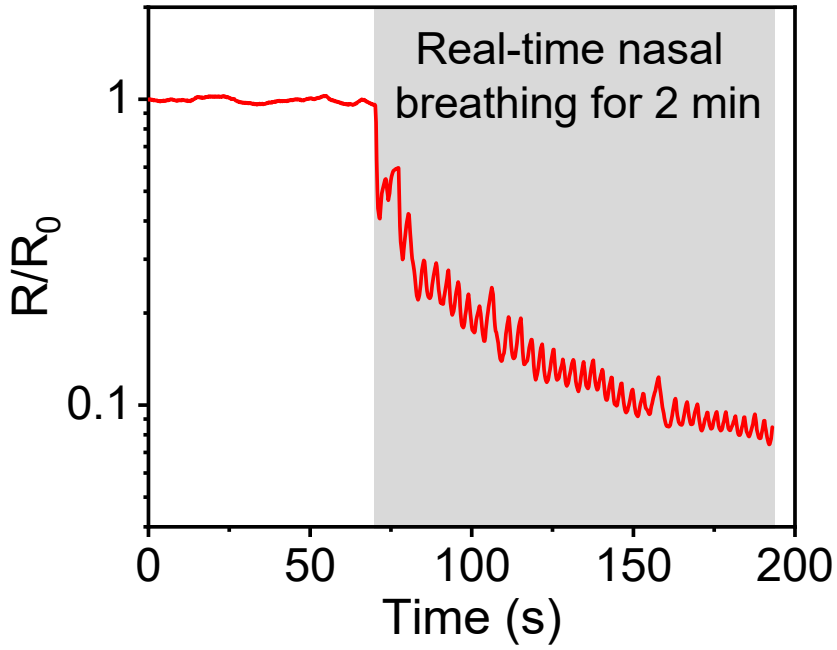

Figure S15 Real-time detection of nasal breathing by the all-cellulose-derived humidity sensor (RH: 24%).

The all-cellulose-derived humidity sensor was applied for real-time nasal breath monitoring. While the decreasing trend of the R/R_0 value during nasal breathing was observed possibly due to the accumulated water vapor within the sensor (possibly because of its low recovery rate), small response and recovery peaks could be clearly detected by every breath. The number of breaths over the 2-min period was 36 (respiratory rate: 18 breaths min^{-1}), which is in line with the normal range of breathing for a healthy adult at rest (12-20 breaths min^{-1}).[7] Thus, the all-cellulose-derived humidity sensor demonstrated sufficient response and recovery enough to monitor nasal breathing.

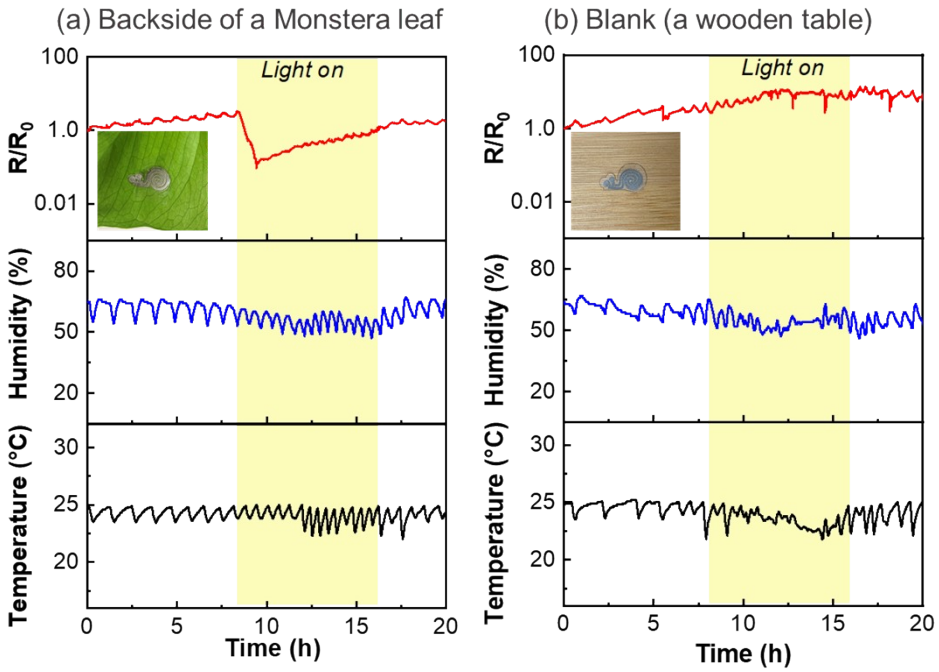

Figure S16 Monitoring of the resistance of all-cellulose-derived humidity sensors attached to (a) the backside of a *Monstera* leaf and (b) a wooden table, and monitoring of atmospheric humidity and temperature by a commercial sensor.

Transpiration is an important biological process for plants. This process converts liquid water absorbed by the roots of the plant to water vapor through the stomata. Most stomata for terrestrial plants are distributed on the backsides of leaves. Transpiration is enhanced by visible light illumination because the density of opened stomata increases when the leaf is exposed to visible light.[8] To monitor the transpiration process in plants, we attached our humidity sensor to the backside of a *Monstera* leaf (**Figure S16a**), and to a wooden table for comparison (**Figure S16b**). Upon visible light illumination, the resistance of the sensor attached to the leaf clearly decreased, while that attached to the wooden table did not. Atmospheric humidity and temperature were steady during this experiment, indicating that the sensor detected water vapor from the leaf via the transpiration process.

Table S1 Sensing performances of state-of-the-art cellulose-based humidity sensors

Sensing material	Electrode	Relative humidity range	Sensitivity	Response/ recovery time	Ref.
TEMPO-oxidized cellulose nanofibril/ single-walled nanotube	no	50-95%	-	-/-	9
TEMPO-oxidized cellulose fiber/ carbon nanotube	no	11-95%	*ca.* 2.17×10^3	333/523 s	10
TEMPO-oxidized cellulose nanofibril	Graphene	20-90%	*ca.* 1.50×10^5	200/1020 s	11
TEMPO-oxidized cellulose nanofibril/ poly(ethylene glycol)			*ca.* 1.32×10^4	265/490 s	
A4 printing paper	Cu−Ni alloy	7.2-91.5%	*ca.* 4.80×10^3	19/472 s	12
Multi-walled carbon nanotube/hydroxy-ethyl cellulose	Silver	20-80%	*ca.* 8.00×10^1	20/35 s	13
Oxidized multiwalled carbon nanotubes/ cellulose paper	Graphite	11-95%	-	5−8/ 7−11 min	14
Carboxymethyl cellulose	Carbon fiber	10-60%	-	< 5 min/-	15
TEMPO-oxidized cellulose fiber	Laser-carbonized cellulose	11-98%	1.19×10^5	60/495 s	This study

Note: The sensitivity (S) was calculated from the response and recovery curve by the equation: $S = \Delta R/\Delta RH$, where ΔR is the change in sensor resistance and ΔRH is the change in relative humidity level. [16]

References

1 T. Saito and A. Isogai, *Biomacromolecules*, 2004, **5**, 1983–1989.

2 K. Lichtenstein and N. Lavoine, *Polym. Degrad. Stab.*, 2017, **146**, 53–60.

3 H. Fukuzumi, T. Saito, Y. Okita and A. Isogai, *Polym. Degrad. Stab.*, 2010, **95**, 1502–1508.

4 J. Lin, Z. Peng, Y. Liu, F. Ruiz-Zepeda, R. Ye, E. L. G. Samuel, M. J. Yacaman, B. I. Yakobson and J. M. Tour, *Nat. Commun.*, 2014, **5**, 5–12.

5 W. Zhang, D. Jiang, Z. Guo, X. Yang, N. Hu, Y. Duan, S. Gao, Q. Liang, T. Zheng and J. Lv, *Superlattices Microstruct.*, 2018, **115**, 177–182.

6 A. De Luca, S. Santra, R. Ghosh, S. Z. Ali, J. W. Gardner, P. K. Guha and F. Udrea, *Nanoscale*, 2016, **8**, 4565–4572.

7 F. Güder, A. Ainla, J. Redston, B. Mosadegh, A. Glavan, T. J. Martin and G. M. Whitesides, *Angew. Chemie - Int. Ed.*, 2016, **55**, 5727–5732.

8 Y. Lu, K. Xu, L. Zhang, M. Deguchi, H. Shishido, T. Arie, R. Pan, A. Hayashi, L. Shen, S. Akita and K. Takei, *ACS Nano*, 2020, **14**, 10966–10975.

9 H. Koga, T. Saito, T. Kitaoka, M. Nogi, K. Suganuma and A. Isogai, *Biomacromolecules*, 2013, **14**, 1160–1165.

10 P. Zhu, Y. Kuang, Y. Wei, F. Li, H. Ou, F. Jiang and G. Chen, *Chem. Eng. J.*, 2021, **404**, 127105.

11 T. Syrový, S. Maronová, P. Kuberský, N. V Ehman, M. E. Vallejos, S. Pretl, F. E. Felissia, M. C. Area and G. Chinga-carrasco, *J. Appl. Polym. Sci.*, 2019, **136**, 47920.

12 Z. Duan, Y. Jiang, M. Yan, S. Wang, Z. Yuan, Q. Zhao, P. Sun, G. Xie, X. Du and H. Tai, *ACS Appl. Mater. Interfaces*, 2019, **11**, 21840–21849.

13 V. S. Turkani, D. Maddipatla, B. B. Narakathu, T. S. Saeed, S. O. Obare, B. J. Bazuin and M. Z. Atashbar, *Nanoscale Adv.*, 2019, **1**, 2311–2322.

14 H. Zhao, T. Zhang, R. Qi, J. Dai, S. Liu and T. Fei, *ACS Appl. Mater. Interfaces*, 2017, **9**, 28002–28009.

15 R. Barras, I. Cunha, D. Gaspar, E. Fortunato, R. Martins and L. Pereira, *Flex. Print. Electron.*, 2017, **2**, 014006.

16 Y. Wang, S. Hou, T. Li, S. Jin, Y. Shao, H. Yang, D. Wu, S. Dai, Y. Lu, S. Chen and J. Huang, *ACS Appl. Mater. Interfaces*, 2020, **12**, 41896–41904.